Journal of Structural Geology 33 (2011) 731–742

Contents lists available at ScienceDirect

Journal of Structural Geology

journal homepage: www.elsevier.com/locate/jsg

Influence of combined incision and fluid overpressure on slope stability: Experimental modelling and natural applications

Aurélien Lacoste [a,*], Bruno C. Vendeville [a], Lies Loncke [b]

[a] UMR 8157 Géosystèmes, Université de Lille 1, Bâtiment SN5, 59655 Villeneuve d'Ascq Cedex, France
[b] Université de Perpignan, Via Domitia, Laboratoire IMAGES, Bat U, 2e étage, 52 avenue Paul Alduy, 66800 Perpignan, France

ARTICLE INFO

Article history:
Received 11 September 2009
Received in revised form
14 January 2011
Accepted 29 January 2011
Available online 1 March 2011

Keywords:
Landslides
Fluid overpressure
River incision
Analogue modelling

ABSTRACT

Onshore slides are driven by gravitational forces that are either related to a basal or a surface slope. Resisting these driving forces are the friction at the base of the slide, and the strength to compressional failure at the downslope edge of the slide. Two distinct processes can reduce these resisting forces and thereby promote slides. On one hand, fluid overpressure at the base of low-permeability layers decreases the effective stress, shifting the Mohr circle closer to the failure envelope. On the other hand, river incision removes the downslope buttresses. We undertook analogue experiments to investigate the combined influence of both processes on promoting landsliding. We applied air pressure at the base of horizontal or tilted models made of high and low-permeability layers to induce basal overpressure, combined with local incision similar to river incision in nature. We also tested the differences in deformation as a function of whether the incision was continuous throughout the models' evolution.

No deformation occurred in the regions not subjected to overpressure. In models subjected to continuous incision, normal faults formed first along the valley flanks, then propagated upslope retrogressively. Where incision was not continuous through time, a downslope buttress progressively formed with the sliding mass comprised of an extensional domain upslope, a long, translated but non-deformed slab at mid-slope, and a shortened domain downslope. In our models, the size of the deformed area increased with incision depth and/or increasing basal slope. These results show that river incision, combined with fluid overpressure is a potential landslide-triggering factor, as suggested by field data gathered at the Waitawhiti landslide complex, North Island, New Zealand.

1. Introduction

A slope instability requires that the driving force (the slope-parallel component of the weight along the sliding section) must exceed the two forces resisting deformation: the frictional force along the slope-parallel sliding plane, and the force resisting shortening at the base of the slope (Terzaghi, 1959). The first resisting force can be reduced by the presence of overpressured fluids. Fluids accumulating at the base of low-permeability layers induce a critical decrease in effective stress (Terzaghi, 1923; Hubbert and Rubey, 1959; Mourgues and Cobbold, 2003, 2006), and therefore can generate gravitational slides (Amazon deep-sea fan, Cobbold et al., 2004; Niger delta, Weber and Daukoru, 1975; Hooper et al., 2002; "Storegga slide", Kvalstad et al., 2005).

Rising fluids, such as water, methane or hydrogen, can easily be detected in marine environments when they reach the surface, forming pockmarks or gas chimneys. The development of high-resolution tools, such as seismic reflection, well logging and bathymetric imagery, has revealed frequent associations between fluids originating at depth and the onset of submarine mass movements (Hovland et al., 2002; Gay et al., 2004; Lastras et al., 2004; Loncke et al., 2004; Sultan et al., 2004; Trincardi et al., 2004; Bayon et al., 2009).

By contrast, when dealing with instabilities located onshore, the traditional approaches consider only meteoric fluids. Intense rainfall and subsequent subsurface water flows lead to increased pore-fluid pressure, reducing the effective stress along hillslopes (Binet et al., 2007) and causing landsliding (e.g., Taïwan, Chen et al., 2006). Rainfall-induced landsliding may be enhanced by the presence of clay-rich layers (e.g., swelling clay, such as smectite) that can act as very efficient décollement layers (Shuzui, 2001). On one hand, swelling of the clay-rich layers induces a pervasive decrease in the mechanical strength, and sliding takes place *on* or *near the top* of these layers. On the other hand, overpressured fluids originating at depth and migrating upward can cause a drastic reduction in the effective stress *along the base* of low-permeability layers, which

* Corresponding author. Tel.: +33 3 20434692; fax: +33 3 20434910.
E-mail address: aurelacoste@gmail.com (A. Lacoste).

0191-8141/$ – see front matter © 2011 Elsevier Ltd. All rights reserved.
doi:10.1016/j.jsg.2011.01.016

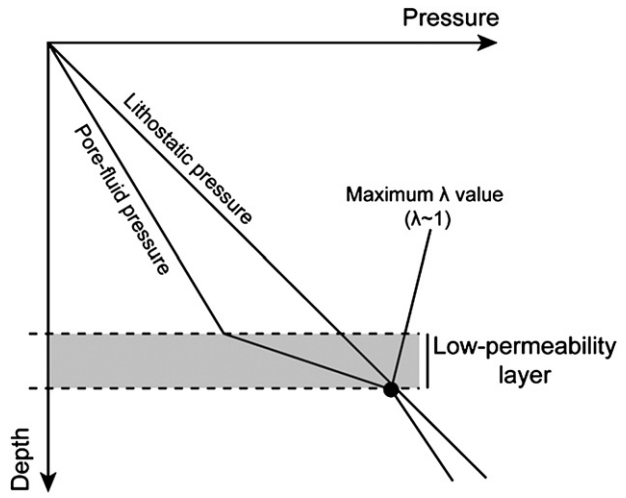

Fig. 1. Theoretical diagram showing change with depth in the lithostatic and pore-fluid pressures. Note that the coefficient of fluid pressure (λ) reaches maximum values at the base of low-permeability layers, where the two pressures are equal (Mourgues and Cobbold, 2003).

then can act as a very sharp detachment (Osborne and Swarbrick, 1997; Mourgues and Cobbold, 2003, 2006).

Recent work by Lacoste et al. (2009) documented the presence of onshore landslides associated with gas seeps and river incisions. They proposed that overpressured fluids originating at depth could be one of the main instability factors controlling this area. However, onshore study of fluids originating at depth and rising to the surface is more complicated than in submarine environments. The observation of the fluid seeps is only possible with the sparse occurrence of mud volcanoes, or in water-filled ponds and streams. Furthermore, monitoring fluid overpressures and their links with landsliding would require time, as ongoing activity of sliding was not clearly attested in the field (Lacoste et al., 2009), and additional logistics, such as piezometers and fluid sensors, whose maintenance would be costly, due to their location in remote streams subjected to seasonal flooding and livestock damage. One approach is to complete detailed field analyses and to determine the potential role of such fluids on landslides by coupling field observations with numerical and/or physical modelling.

The second type of force resisting deformation is the resistance to shortening in the downslope part of the slided mass. Schultz-Ela and Walsh (2002) and Azañon et al. (2005) showed that the removal of distal buttresses by river incision decreases the resisting force downslope and can be an important predisposing factor for gravitational slides. These authors showed that gravitational motion initiated where the river has incised down to potential *décollement* layers (evaporites or shale).

In the Coastal Ranges of the North Island of New Zealand, in the Waitawhiti area, Lacoste et al. (2009) suggested that a strong link exists between landslides, fluvial incision and fluid overpressure. However, on the sole basis of field data, it remains difficult to prove unequivocally that such a link exists. We therefore tested this hypothesis using a series of analogue experiments to delineate the respective roles of combined incision and fluid overpressure on the triggering, structure pattern and evolution of landslides. We then compared the models to natural onshore and marine prototypes, and discussed the influence of combined incision and fluid overpressure on these slides.

2. Scaling

Small-scale models require scaling of the different parameters controlling deformation. The dimension and time ratios between the natural prototype and the experimental model must be constant (Hubbert, 1937; Ramberg, 1981). In this work, we constructed models made of porous, near cohesionless granular materials (quartz sands and glass microbeads) that all obey a Mohr-Coulomb deformation criterion, a frictional-plastic rheological behaviour independent of time and strain rate.

For a brittle model to be properly scaled, it suffices that the density and angle of internal friction be similar in nature and model, and that the value of the cohesion be negligible compared with the other stresses, including gravity, in both models and nature. The mechanical effect of pore-fluid pressure was modelled by injecting a constant flux of compressed air at a precalculated pressure at the model's base. An increase in fluid pressure leads to an increase in the coefficient of fluid pressure (λ) (or Ru). The coefficient of fluid pressure is defined, for any given depth, as the ratio between the fluid pressure and lithostatic pressure, $\lambda = 0$ meaning that fluid overpressure is absent (Fig. 1):

$$\lambda = \left(P_f(z) - P_f(0)\right) \Big/ \rho g z$$

A model is properly scaled for fluid pressure if the value of the coefficient of fluid pressure is similar in nature and model at proportionally equivalent depths. Prior to constructing the models, we calculated the layer thickness required to reach a coefficient of fluid

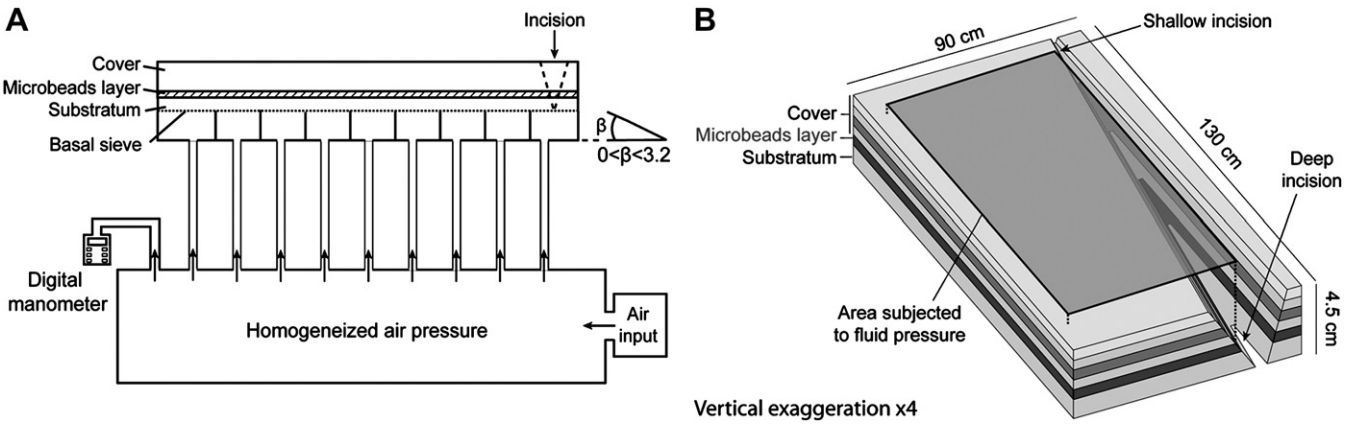

Fig. 2. Experimental set-up. (A) Schematic cross section view of the experimental set-up. (B) 3D view of the models showing differential incisions and the area subjected to fluid pressure.

pressure (λ) nearing 1. We made sure that the lithostatic pressure would not be too low to prevent blowouts of the model that occur when the fluid pressure exceeds the lithostatic pressure, as observed by Mourgues and Cobbold (2006). We must emphasize that the scaling procedure of such models does not account for time or flow rates (Mourgues and Cobbold, 2006). Instead, we scaled our models in terms of the coefficient of fluid pressure, λ, rather than actual flow rate. We then calculated the air pressure used in the lab to reach a λ equivalent to that in nature. For example, λ of 1 is reached in nature for about 800 kPa (for a 40 m-thick cover of density 2000 kg m^{-3}) and about 800 Pa for a model's cover 2.5 cm thick and having a density of 1600 kg m^{-3}. Note that deformation was not continuous through time, occurring only where a certain fluid pressure was applied, depending on the initial boundary conditions.

3. Experimental set-up

The experimental set-up was developed by Mourgues and Cobbold (2006). The models were built on a sieve subjected to fluid pressure (Fig. 2A). In the experiments, we simulated the generation of thermogenic gases using compressed air applied at the base of the model (Fig. 2A). The air pressure was measured using a digital manometer. Our models comprised a 2 cm coarse sand substratum layer (grain size = 316 μm; permeability = 100×10^{-12} m^2), overlain by a 0.5 cm low-permeability layer of glass microbeads (grain

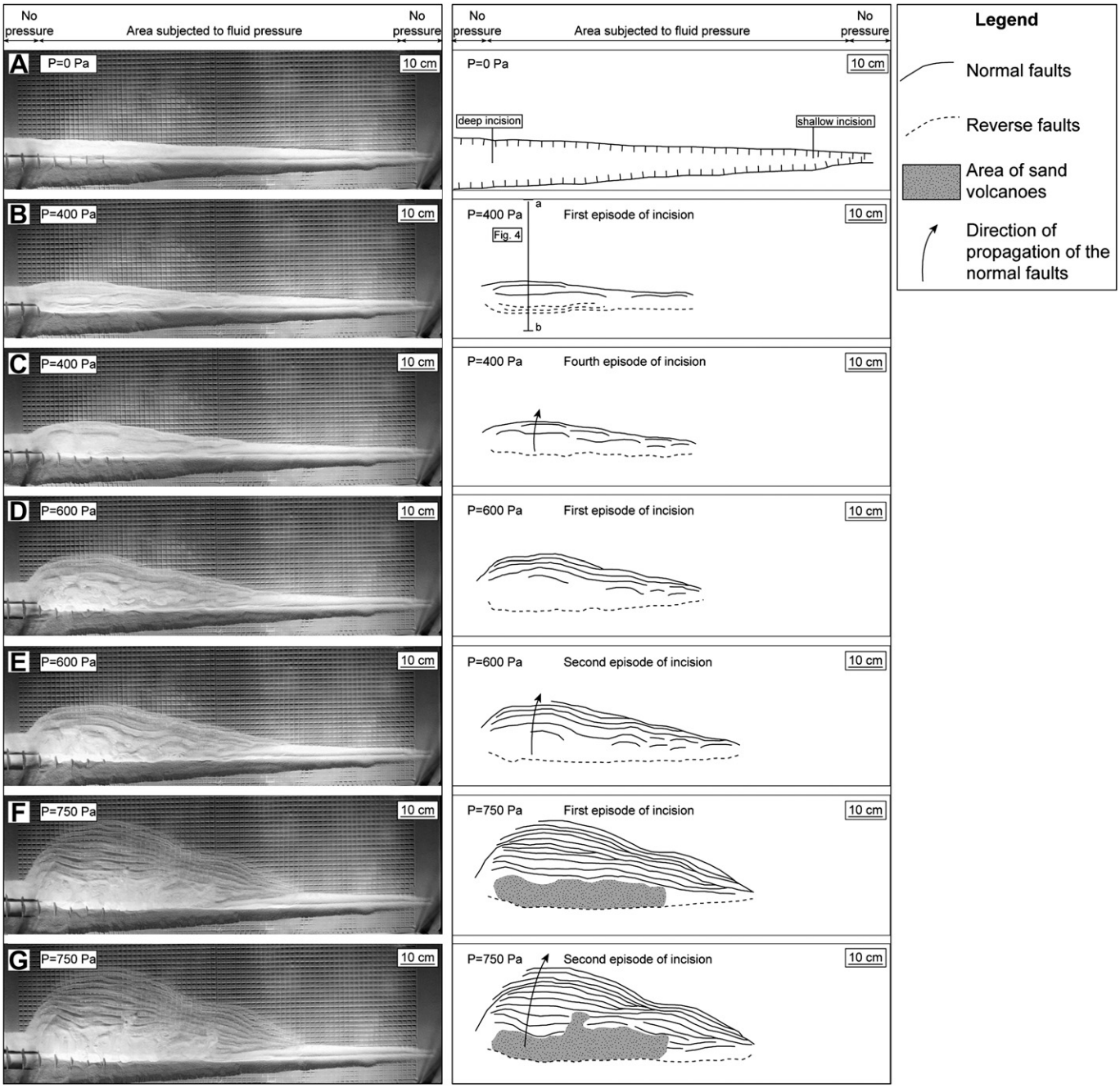

Fig. 3. Overhead photographs (left) and line drawings (right) of model CI-0°. (A) initial stage; (B–C) under 400 Pa air pressure; (D–E) under 600 Pa air pressure; (F–G) under 750 Pa air pressure. For each value of air pressure, several episodes of incision were conducted, removing the downslope buttress in the valley, until no more sliding occurred.

size = 106 μm; permeability = 10×10^{-12} m^2) layer (Fig. 2). We used the microbeads to model a low-permeability layer. A coarse sand cover (grain size = 316 μm; permeability = 100×10^{-12} m^2), composed of four 0.5 cm thick layers overlaid the microbeads. Because of the high permeability of the lower layer of coarse sand, resistance to upward air flow was limited there, hence the air pressure decreased. Whereas, within the low-permeability *décollement* layer, resistance to air flow was greater and the air pressure dropped rapidly. As demonstrated by Mourgues and Cobbold (2006), such configuration leads to values of the lithostatic stress and fluid pressure closest to each other at the base of the low-permeability layer, thus promoting gravity sliding.

Models were 130 cm long, 90 cm large, and were built on a horizontal or tilted base, with or without a valley incision (Fig. 2). The depth of the incision varied laterally from 0 to 4.5 cm (Fig. 2B), and locally intersected the low-permeability layer (glass microbeads) acting as a potential *décollement* layer.

We performed three series of experiments. Each series comprised three models, corresponding to three different basal slopes: 0, 1.6 and 3.2°, respectively. The air pressure was measured and recorded every second during the experiments. In this article, we only present the experiments having the minimum (horizontal) and maximum (3.2°) basal slopes, respectively. The models having an intermediate basal slope yielded results similar to the models having the steepest basal slope, so they are not described.

3.1. Non-incised models (series 'NI')

No incision was initially induced in these series. The air pressure was simply raised at the base of the model until deformation occurred. We used these models as reference models for the study of the influence of incision on sliding.

3.2. Incised models (series 'CI' and 'NCI')

We locally vacuumed the sand cover to model differential incision (Fig. 2B) as an initial boundary condition in these series of experiments. In the first series of incised models (series 'CI'), air pressure was raised until the frictional resistance at the base of the microbeads layer decreased enough to allow the cover to slide (initial sliding pressure threshold: $P = 400$ Pa). We then stopped the experiment, stopped the air flow and physically vacuumed away the slid material along the valley floor. After incising, we then restarted the experiment by progressively and carefully raising the pressure back to its threshold value. This procedure was repeated for several episodes of deformation until no further sliding occurred anymore. We repeated the experimental procedure for different pressure thresholds ($P = 600$ and $P = 750$ Pa).

To avoid interactions between the air pressure applied at the model base and the air flow generated by the vacuum cleaner during incision episodes, we set the basal air pressure to $P = 0$ Pa before each incision episode. This technical constraint had no consequence on the deformation during the experiments because no sliding occurred for pressures being lower than the pressure threshold.

In the series 'NCI', the air pressure was progressively raised until the formation of a contractional toe blocked further sliding. There, unlike during series 'CI', the eroded material was not removed from the valley floor. We then continued to raise the basal air pressure until the model either deformed or exploded.

For each type of set-up, the experiment was conducted several times to ensure that results were reproducible. This protocol also enabled us to cut some cross sections in models at different stages of deformation. In the description of the experimental results, we use the terms "upslope" and "downslope" to refer to the basal slope (hence in a direction perpendicular to the incision), and the terms "upstream" and "downstream" for a direction parallel to the incision.

4. Results

In all experiments, no sliding occurred in the lateral regions, where no air pressure was applied. We also observed that, where deformation occurred, the direction of sliding was perpendicular to the direction of the incision.

4.1. Series 'NI' (non-incised models)

Regardless of the slope inclination, no deformation occurred in models not subjected to incision (series 'NI'). Sand volcanoes developed for pressures reaching $P = 800$ Pa, where the fluid pressure equalled or exceeded the lithostatic pressure. These volcanoes degenerated in large explosions, affecting the whole model, when the pressure was raised.

4.2. Series 'CI' (continuously incised models)

4.2.1. Basal slope = 0° (model CI-0°)

Differential incision was induced, as in natural examples, by removing a shallow part of the cover upstream (right part of the model), and progressively deeper downstream (left part of the model) (Fig. 3A). Normal faults formed on the flank of the valley (Fig. 3B), when the air pressure reached a value of $P = 400$ Pa. A small contractional toe formed on the valley floor (Fig. 3B). After removing the toe, mimicking natural erosion, and applying air pressure again, deformation propagated retrogressively upslope. Fig. 3F illustrates the propagation of the normal faults after multiple incision episodes at pressures of 400 Pa, 600 Pa, and

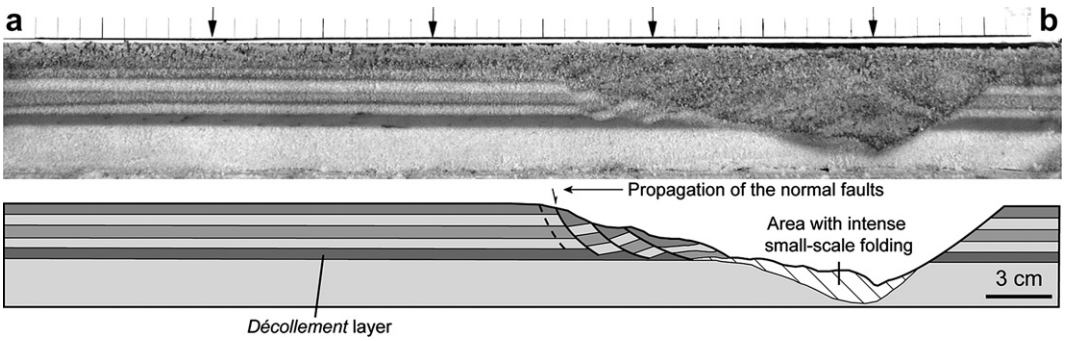

Fig. 4. Photograph (up) and line drawing (down) of a cross section in model CI-0°. See location in Fig. 3B.

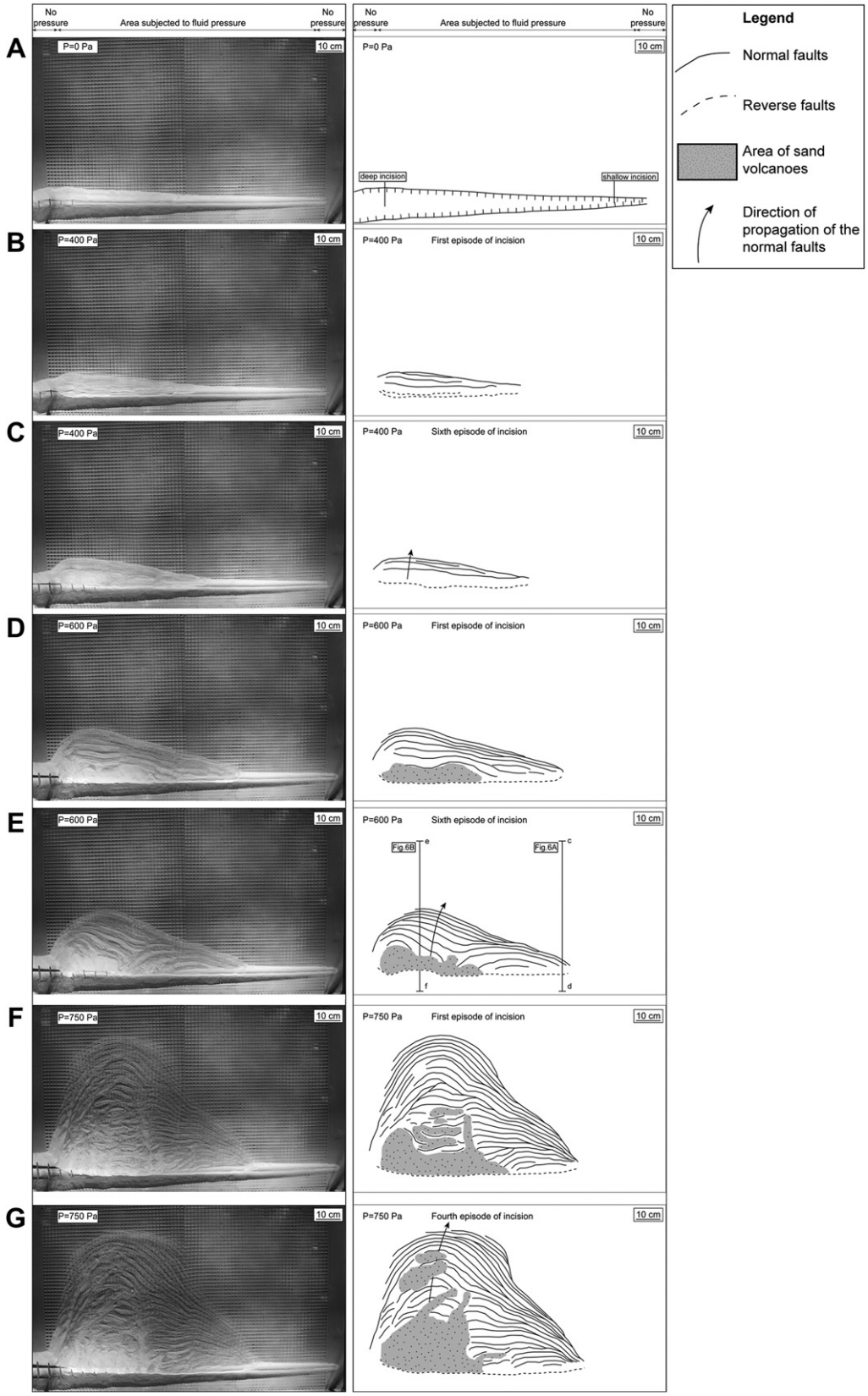

Fig. 5. Overhead photographs (left) and line drawings (right) of model CI-3.2° (basal slope of 3.2°). (A) initial stage; (B–C) under 400 Pa air pressure; (D–E) under 600 Pa air pressure; (F–G) under 750 Pa air pressure. For each value of air pressure, several episodes of incision were conducted, removing the downslope buttress in the valley, until no more sliding occurred.

750 Pa. The number of faults, as well as the area affected by deformation, increased with increasing air pressure (Fig. 3D, E, F and G). During the last episodes, removing the distal toe was sufficient to trigger further sliding without applying greater air pressure (Fig. 3F and G). Sand volcanoes appeared in the vicinity of the incision, complicating the structure of the contractional toe by liquefying part of it. The aerial extent of the deformation was greater in the downstream region, where the incision was deep, whereas no sliding occurred in the rightmost part of the model, where the incision was shallow and did not reach the *décollement* layer (Fig. 3).

Fig. 4 shows a cross section from the beginning of the experiment, deformed at low air pressure values ($P < 400$ Pa). The faults are listric faults rooted at depth into the base of the *décollement* layer. The contractional toe is very complex, characterized by intense small-scale folding and thrusting.

4.2.2. Basal slope = 3.2° (model CI-3.2°)

In this experiment, the entire deformation box was tilted by 3.2° perpendicular to the incised valley. The structural style of these models was similar to that observed in horizontal models (Fig. 5). At constant air pressure, normal faults propagated upslope everytime the downslope buttress was removed. For each pressure value, up to six episodes of incision could trigger sliding, whereas, in model CI-0° (no basal slope), sliding did not occur after four episodes of incision. Comparing the extent of the deformed area in both experiments clearly indicates that, under similar pressure values (e.g., $P = 750$ Pa, Figs. 4F and 5F), deformation in the tilted model is far more widespread than in the horizontal model. The deformed area especially increased greatly in the left part of the model, where the incision was deepest (Figs. 5 and 6). The deformation front propagated upslope up to an area where no air pressure was applied (see Fig. 2B). Presumably, deformation would have propagated further upslope if a wider area had been subjected to air pressure. Sand volcanoes formed in the late stages of deformation. These sand volcanoes were located in the downslope part of the model, in areas where the sedimentary cover was thinned by normal faulting. The contractional domain is characterized by intense small-scale folding and thrusting and is restricted within the incised valley.

Cross sections made at the end of the experiment (Fig. 6) show that normal faults are listric and that their dip decreases for faults positioned nearer incised valley. As in the horizontal model, deformation was greatest in the area located upslope the deepest valley incision (Fig. 6B). Intense and complex deformations also characterize the distal contractional domain (Fig. 6C).

4.3. Series 'NCI' (non-continuous incision)

4.3.1. Basal slope = 0° (model NCI-0°)

In this experiment, the entire deformation box was horizontal, but the frontal buttress (i.e., the contractional toe) generated by

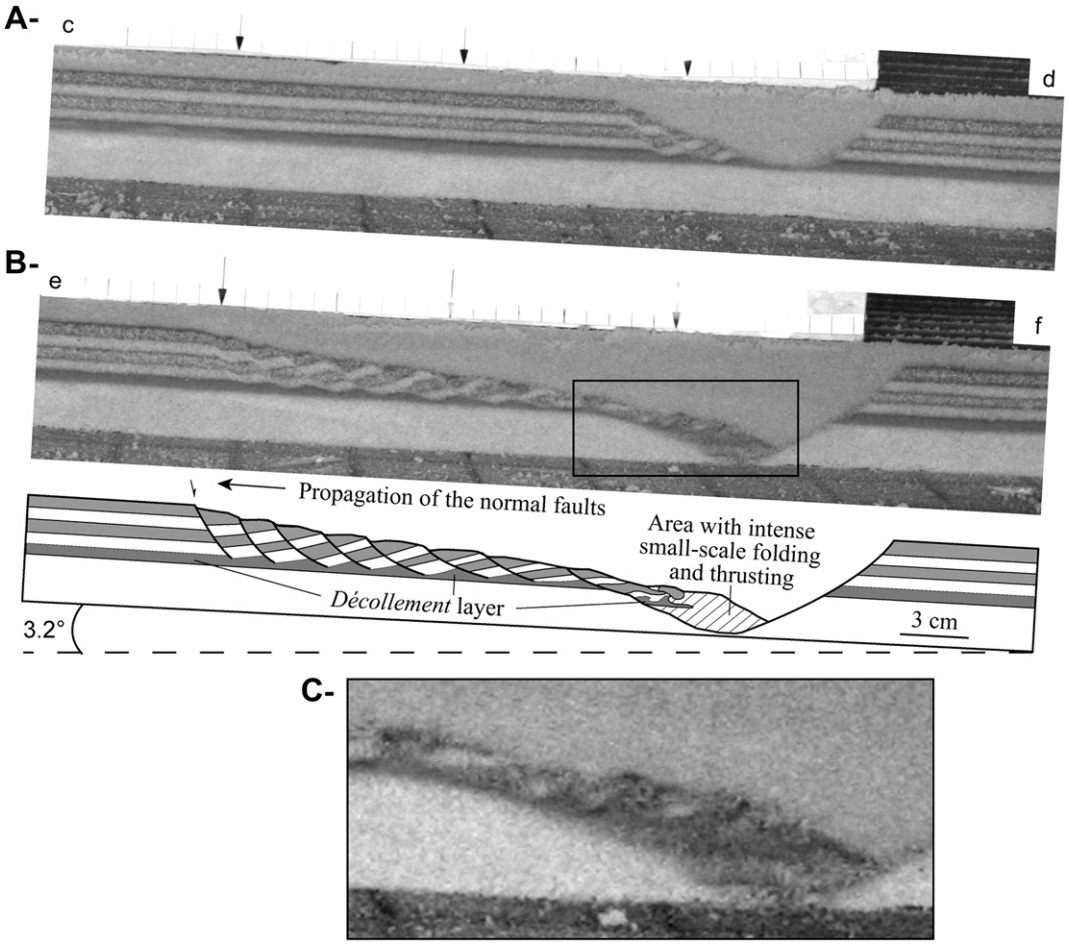

Fig. 6. Cross sections of model CI-3.2°. (A) Photograph of a cross section in the shallow-incised part of the model (upstream). (B) Photograph and line drawing of a cross section in the deeply incised part of the model (downstream). (C) Close-up of the contractional domain in the incised valley. Note that this area is highly deformed by folds and thrusts. Chaotic mixing of the different sand layers makes detailed description of this domain very difficult. See location in Fig. 5.

each sliding episode was not continually removed. Instead, the air pressure was continuously raised in order to enable movement. Normal faults first formed on the valley flanks, then propagated retrogressively with increasing air pressure (Fig. 7B, C and D). Thickening of the downslope contractional toe eventually stopped the retrogressing propagation of normal faults ($P = 800$ Pa, Fig. 7D). The extent of the deformed area was much smaller than in models where the contractional buttress was continuously removed.

When the air pressure reached $P = 800$ Pa, sand volcanoes formed. These volcanoes appeared first on or near normal faults, where faulting had thinned the cover, thereby decreasing the lithostatic pressure and increasing the coefficient of fluid pressure. These sand volcanoes then evolved into large blowouts ($P = 810$ Pa, Fig. 7E) and propagated within the model as pressure increased.

4.3.2. *Basal slope = 3.2° (model NCI-3.2°)*

In this experiment, the entire deformation box was tilted by 3.2° perpendicular to the incised valley, and the frontal buttress generated by each sliding episode was not continually removed. The structural style (Fig. 8) for pressure values $P < 725$ Pa where sliding began to be blocked by the formation of a buttress was the same as in model NCI-0° (horizontal). However, the deformed area

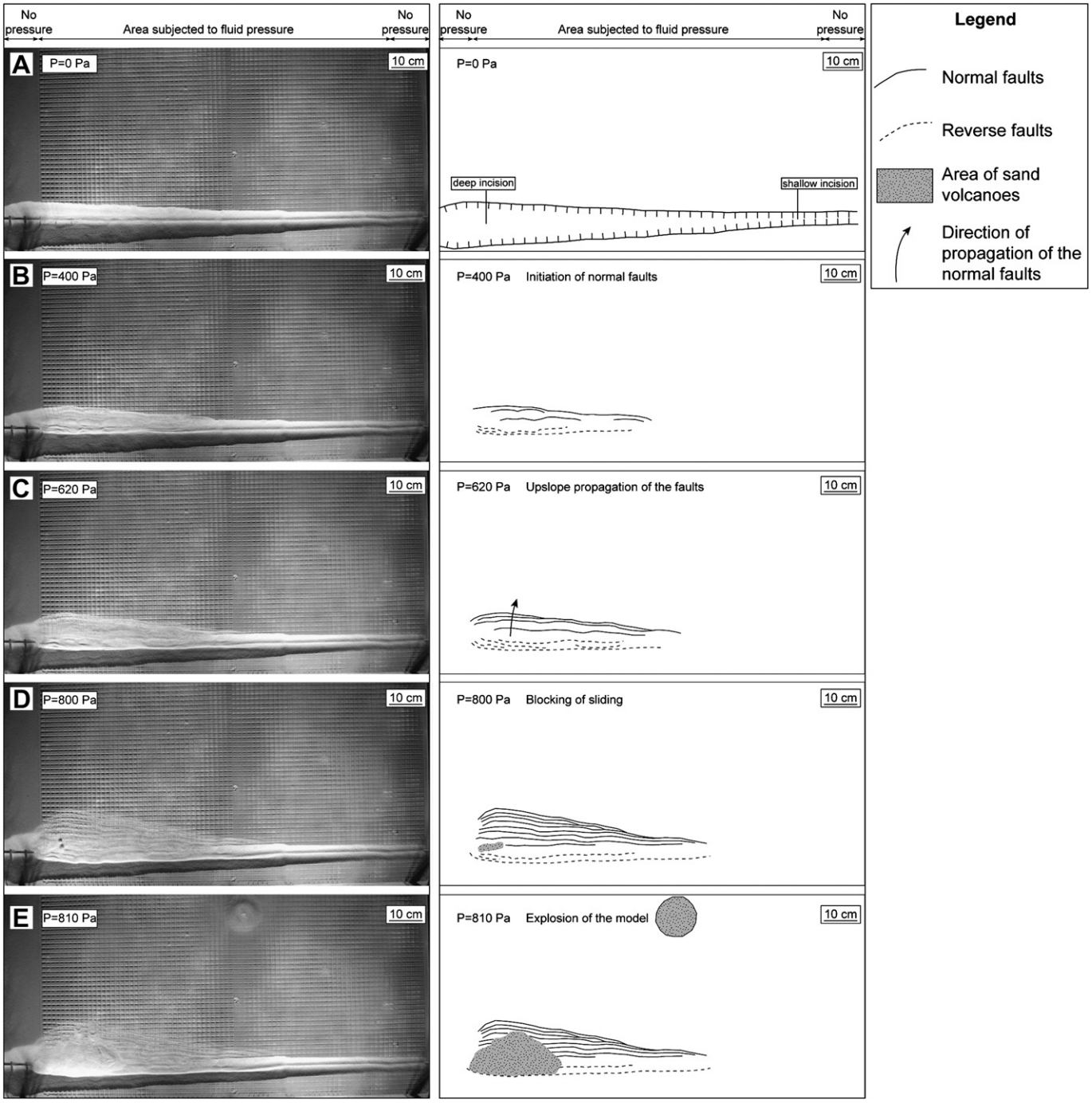

Fig. 7. Overhead photographs (left) and line drawings (right) of model NCI-0° (horizontal base; no removal of the compressional buttress). (A) initial stage; (B) 400 Pa air pressure; (C) 620 Pa air pressure; (D) 800 Pa air pressure; (E) 810 Pa air pressure with occurrence of a large sand volcano.

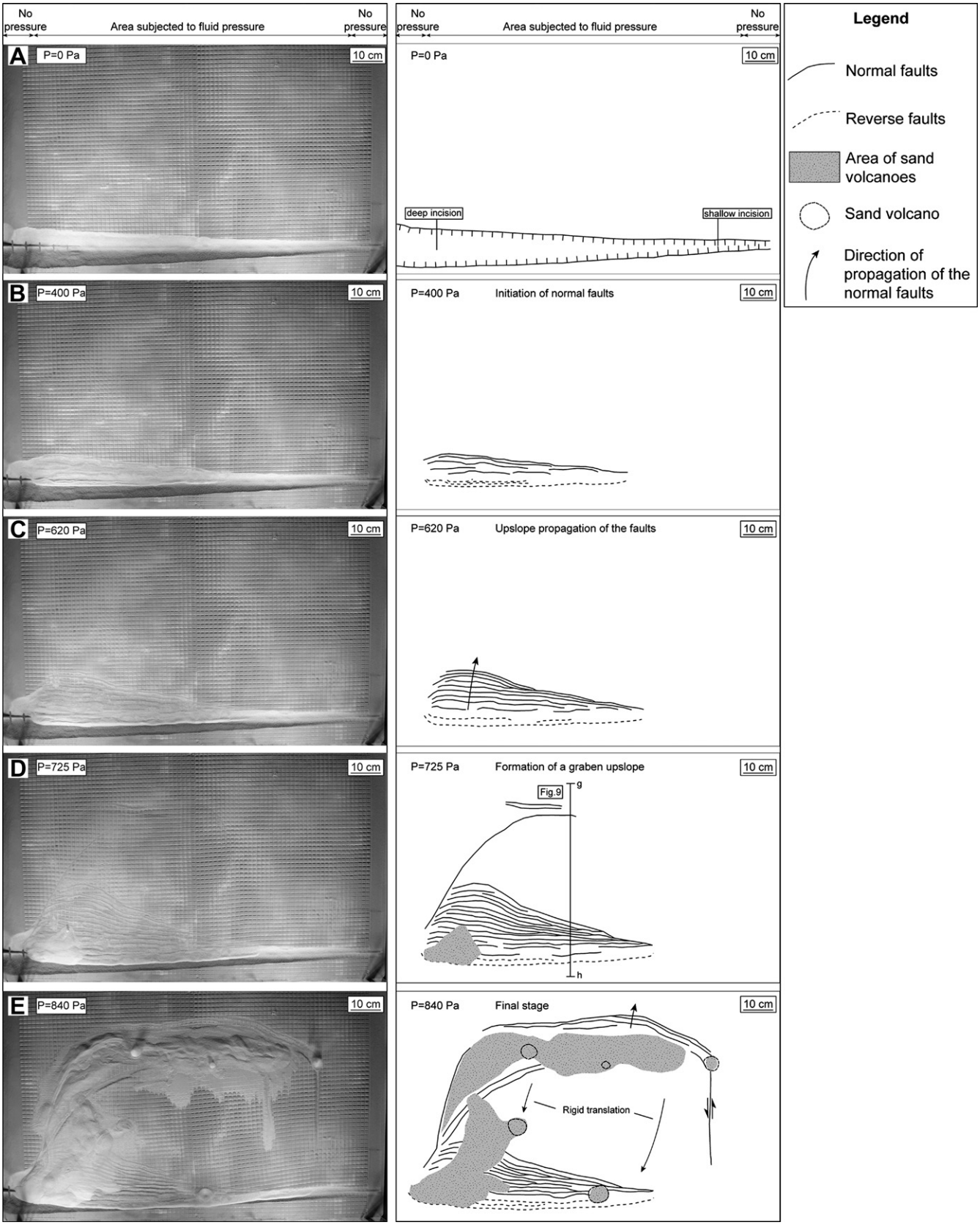

Fig. 8. Overhead photographs (left) and line drawings (right) of model NCI-3.2° (basal slope of 3.2°; no removal of the compressional buttress). (A) initial stage; (B) 400 Pa air pressure; (C) 620 Pa air pressure; (D) 725 Pa air pressure; (E) 840 Pa air pressure with occurrence of numerous sand volcanoes.

was greater than in model NCI-0°. Interestingly, sliding was blocked for pressure values less than those in the experiments NCI-0° ($P < 725$ Pa; Fig. 8D). When the contractional toe blocked sliding, a graben initiated much farther upslope in the model (Fig. 8D), when pressure reached values of $P = 725$ Pa. As fluid pressure increased, the upslope graben and associated normal faults propagated along strike and both upslope and downslope (Fig. 8E). The entire cover slid rigidly towards the incised valley, as a long, non-deformed block. No new faults formed downslope, and deformation was restricted to numerous sand volcanoes.

The boundary between the slid parts of the model and the stable lateral regions (not subjected to fluid pressure) was marked by transtensional faults oriented perpendicular to the valley direction (Fig. 8E). In map view, the traces of normal faults changed laterally and progressively became subparallel to the strike-slip bounding faults. In the area most thinned by normal faulting (upslope from the area where the incision was deepest), sand volcanoes erupted because of normal faulting and ensuing local decrease in lithostatic pressure (Fig. 8E).

The cross section presented in Fig. 9 was cut in a model stopped right after the formation of the upslope graben. It illustrates the presence of listric normal faults in the vicinity of the incised valley. These faults formed in response to the air pressure increase during the first episodes of deformation ($P < 725$ Pa) and later slid rigidly towards the contractional area (the incised valley), pinching-out the contractional toe made of small-scale folds. The planar normal fault located on the left side of the cross section (Fig. 9) formed farther upslope. This fault marks the upslope graben that bounds the large block of cover that was translated rigidly downslope. Past this stage (Fig. 8D), the downslope normal faults were no longer activated.

5. Interpretations – Discussion

5.1. Impact of incision on landsliding

The experimental results described above illustrate the impact that river incision can have on promoting landslides when combined with fluid overpressure. The combination of a low basal resistance related to fluid overpressure, and the lack of downslope buttress reduces the resistance to sliding and can trigger deformation, even where the driving forces proportional to the sedimentary cover thickness and the basal slope angle are only moderate.

No deformation occurred in models where the buttress was present and the driving force was small (series 'NI', horizontal models with no incision). In another series, Mourgues and Cobbold (2006) tested models with a basal slope but without any incision. Their work demonstrated that the models need to reach a minimum length in the motion direction for the driving force, which is the slope-parallel component of the sedimentary cover weight, to overcome the buttressing resistance downslope.

By contrast, in all of our models where part of the cover was removed by river incision, some deformation occurred. Gravitational sliding of the sedimentary cover was accommodated by normal faults that first formed along the valley flanks, then propagated retrogressively upslope. These faults became listric by rotational sliding processes during additional collapse of the cover. It must be emphasized that even models having an incision but no basal slope deformed, albeit to a lesser extent than tilted models, confirming the important control of incision in preparing and triggering mass movement and retrogressive propagation of landslides.

5.2. Landslides structure and evolution

5.2.1. Permanent incision (series 'CI')

The initial incised conditions of these models allowed the valley flank to first slide as pressure reached its threshold value. Subsequently, and for each stage of the experiment, sliding was accompanied by the formation of a small contractional buttress on the valley floor. As it grew, the buttress resistance to sliding increased, which led to a complete stop in deformation, marking the stage where the resisting and driving forces balanced. Then, the air flow was shut while the excess material that had slid into the valley was vacuumed, mimicking natural river erosion. This action successfully removed the frontal resisting force, thus allowing further sliding to occur without even requiring increasing the pressure above its initial threshold. Sliding took place by reactivating and tilting the pre-existing faults and generating new normal faults upslope. The deformed area widened and its extent increased with increasing basal slope angles. Deformation started only near segments of the valley where the incision was deep enough to reach the *décollement* level. The lateral extent of the slid area was controlled by the incision depth. The widest deformed areas were always located upslope of the deepest incisions. Sand volcanoes formed late in response to thinning of the cover and increased fluid pressure. These volcanoes were preferentially initiated along normal faults, where the cover had been thinned most and hence weakened.

5.2.2. Non-permanent incision (series 'NCI')

In these models, the frontal buttress generated by each episode of sliding was never removed. Initially, normal retrogressive faulting developed as the air pressure was raised, as was the case for the series 'CI' models. However, the contractional buttress thickened as more material accumulated on the valley floor, which effectively blocked sliding earlier than in the other experiments. For example, the model having a horizontal basal slope (model NCI-0°), did not

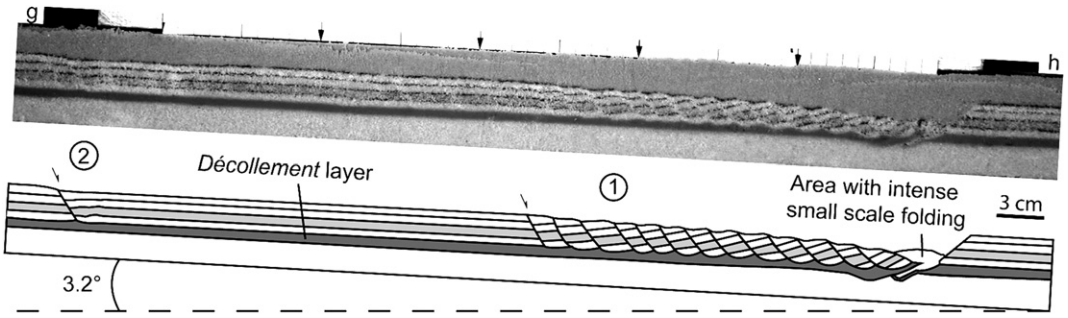

Fig. 9. Photograph (up) and line drawing (down) of a cross section in model NCI-3.2°. (1) The listric normal faults formed in the downslope area during the first episode of the experiment ($P < 725$ Pa). (2) The upslope normal fault formed when the compressional toe blocked sliding. See location in Fig. 8D.

deform anymore after the first event of sliding was blocked, even when the air pressure was increased. Instead, sand volcanoes formed that led to large explosions as the air pressure was raised (Fig. 7E). In the tilted model NCI-3.2°, we observed four structural domains within the slid mass from the valley floor to the upslope area: (1) a contractional domain infilling the valley, (2) a densely faulted area comprising many listric normal faults – some even occupying a part of the incised valley, (3) a non-deformed area translated rigidly above the *décollement* layer and (4) grabens and normal faults in the upslope areas (Fig. 8E).

This model evolution shows a transition in structural style between a non-buttressed sliding system with normal faulting progressing from the valley flank upslope to a buttressed system with rigid translation of a large block or the cover. Comparison between the permanent and non-permanent incision models reveals that not only can initial incision trigger a sliding event, but that continuous incision affects the evolution of deformation by promoting additional sliding, affecting a wider area without any increase in fluid pressure, whereas a lack of continued incision eventually stops sliding.

5.3. Influence of the basal slope

In our models, the only driving force is the gravitational force depending on the weight of the sliding mass. Where there was no basal slope (models CI-0° and NCI-0°), the driving force was small. Although a first sliding event took place, it quickly was blocked when reaching an equilibrium surface slope in model CI-0° and when the downslope buttress grew thick enough in model NCI-0°. No further sliding occurred, even when the basal fluid pressure was raised. Overall, only an area located in the vicinity of the incised valley deformed.

This behaviour changed if a basal slope was added (models CI-3.2° and NCI-3.2°). In this set-up, the driving force was the slope-parallel component of the weight of the entire cover, which was much greater than in horizontal models. The deformed area was wider, and increased as fluid pressure increased. In the case of model having no permanent incision (model NCI-3.2°), the driving force was still sufficient to overcome the frontal resistance exerted by the growing downslope buttress and allowed for massive rigid translation of the entire cover till the end of the experiment. Comparison between horizontal and tilted models thus indicates that, although a basal slope is not necessary, it significantly enhances the areal extent, longevity, and deformation in the slides.

6. Applications: onshore landsliding, the Waitawhiti landslides (Lacoste et al., 2009)

6.1. Morphological and structural characteristics

The Waitawhiti area is the site of a 5-km^2 landslide complex (Fig. 10) located in the Coastal Ranges of the North Island of New

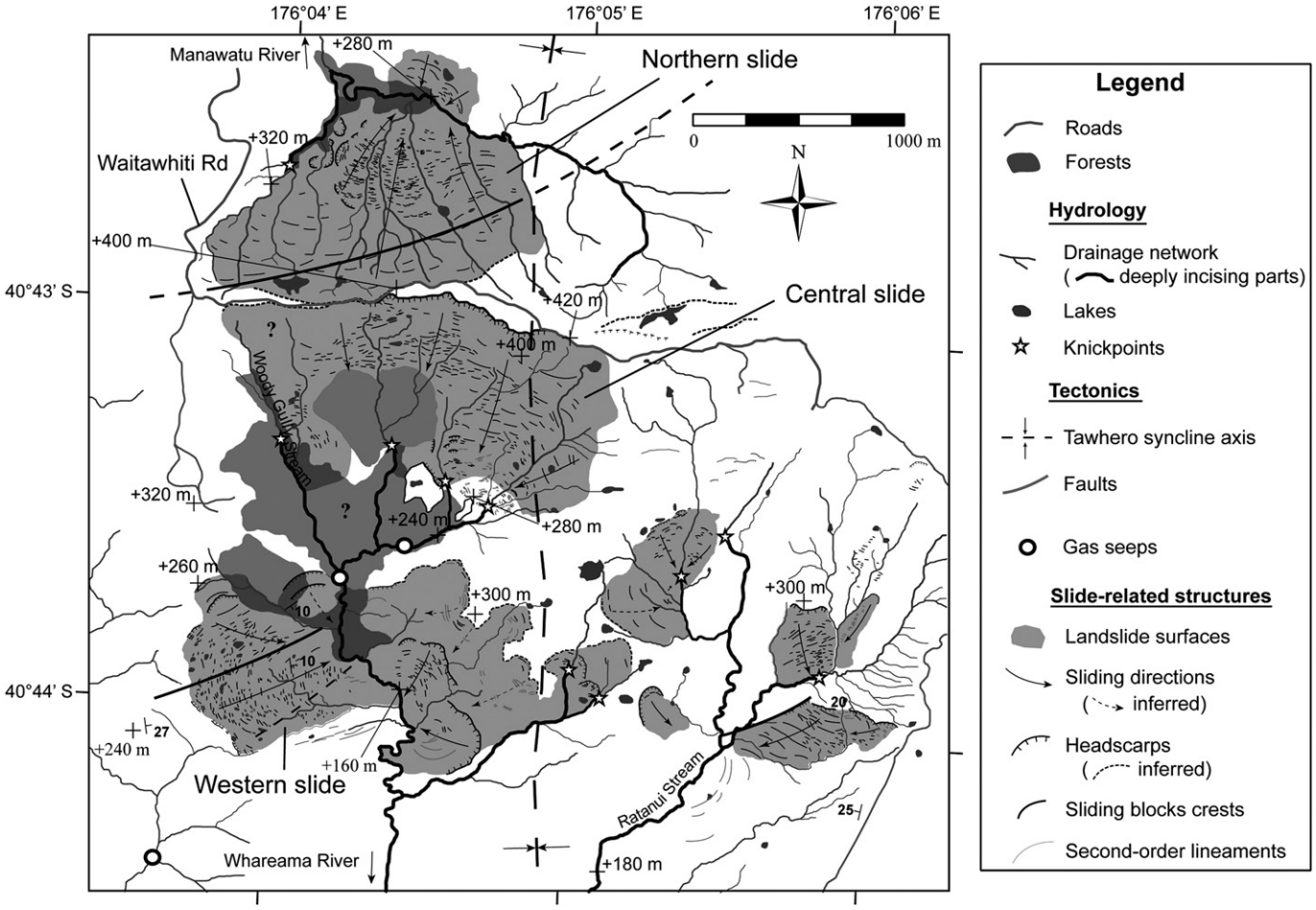

Fig. 10. Morphostructural map of the Waitawhiti area based on QuickBird satellite image interpretation and field work. Note that all slides are bounded distally by incised valleys (drainage network in bold) and occur for different stratigraphic dips (see syncline axis for reference) and surface slope values (modified after Lacoste et al., 2009).

Zealand. Lacoste et al. (2009) identified postglacial fluvial incision as the main destabilizing factor in this area. Deep incisions cause the removal of downslope buttresses, thus regularly activating the slides through time. However, Lacoste et al. (2009) also related the Waitawhiti landslides to other possible preparatory or triggering factors, such as earthquakes, rainfall and, more originally, to fluid overpressure. Indeed, three gas seeps were mapped within the Waitawhiti landslide complex (Fig. 10). These methane gas seeps occur from the upward migration of thermogenic gases in the region, possibly inducing fluid overpressure at the base of low-permeability, clay-rich layers identified in the field (Lacoste et al., 2009).

The main characteristics of the Waitawhiti landslides are that they are bounded downstream by deeply incised valleys. These slides are multi-directional and some of them affect very low slope-gradient topographies (see Lacoste et al., 2009, for complete review). The sliding directions are generally perpendicular to the river pathways (Fig. 10), which suggests that the primary control on landsliding is incision. The northern and central Waitawhiti slides (Fig.10) affect horizontal stratigraphic series, whereas rocks on the western flank of the syncline involved in the western slide are tilted by as much as 20°. The surface slopes of the Waitawhiti landslides vary from less than 5° in the western slide to 11° in the central and northern slides. Lacoste et al. (2009) also showed that the layers forming the base of the slides have a high clay content, dominated by smectite. When subjected to fluid overpressure, these low-permeability layers may thereby act as *décollement* layers for the slides. Finally, the Waitawhiti landslides only show evidence for extensional, normal faulting. No examples of rigid translation of long, non-deformed blocks occur. In addition, no compressional downslope structures were found in the Waitawhiti area, except in one small, local spot, at the toe of the northern slide (Lacoste et al., 2009).

6.2. Role of fluid overpressure combined with river incision

A comparison between the structural style developed in our models and observed in the Waitawhiti area does not prove, as monitoring of actual slides would be necessary, but supports the hypothesis that fluid pressure combined with river incision is the potential triggering factor for these slides. In our experiments involving permanent incision (series 'CI'), the continuous removal of the contractional toe promotes sliding, even on very gentle slopes, as is the case for the northern and central slides, located in the core of a syncline (Fig. 10). The process of permanent incision explains the absence of contractional domain in the Waitawhiti area by erosion, except very locally, where it has not been eroded entirely by river incision. Furthermore, normal faults in the series 'CI' experiments propagated from the valley flanks upslope. After the models were subjected to sufficient fluid pressure to trigger landsliding, episodes of incision, removing the contractional domains that formed, allowed for regular reactivation of the slides. Therefore, two processes could account for the ongoing activity of the Waitawhiti landslides: (1) in the case of constant fluid pressure, regular seasonal incision episodes could induce landsliding progressing from the valley flank upslope; or (2) if incision is not constant through time, increases in fluid pressure would propagate sliding farther upslope.

6.3. Potential role of water table

In our approach, we focused on the influence of fluids forming at depth (methane gas) and migrating upward until they accumulate beneath low-permeability layers, as is the case in our natural example. The presence of these fluids reduces the effective stress, hence the overall resistance to shear stress, along the base of the low-permeability layer, and thereby makes it easier for the overlying layers to slide under gravitational force.

To some extent, the same reasoning could be applied to the influence of fluids of other origin, such as meteoric water, although the mechanics may differ slightly. While methane gas is produced at depth, migrates *upward*, and becomes trapped *beneath* low-permeability layers, rain water would migrate *downward* until it is trapped *above* low-permeability layers. There, the effect of the water table would be two-fold. First, the average density of porous rocks would increase, thus increasing the force driving sliding. Second, the buoyancy forces related to water's density would reduce the effective stress. The main difference with our model would be that, in this case, the level where the pore-fluid pressure would be closest to the lithostatic stress, hence the resistance to shear would be the lowest, would be located *at the top*, rather than at the base, of the low-permeability layers. Sliding would thus take place along the top of the low-permeability layers, which is not the case in the Waitawhiti landslide complex.

7. Conclusions

We performed analogue experiments to investigate the combined effect of incision and fluid overpressure on landsliding, an effect that is extremely difficult to measure or even observe in the field, even when it is suspected to be present. Models having no fluid overpressure did not deform. Even when subjected to fluid pressure, models did not deform unless their downslope area was incised deeply enough to reach the *décollement* layer. The extent of the deformed areas increased with increasing fluid pressure, increasing depth of incision, and increasing basal slope angle.

Our experimental results demonstrate that river incision is a parameter complementary to fluid overpressure for promoting landsliding by critically reducing the resisting forces. While fluid overpressure reduces the effective stress at the base of the slide, river incision removes the frontal buttress that may otherwise resist motion.

Although the above observations apply to all models, the structural evolution of our models greatly varied as a function of whether river incision continued through the entire model history, as opposed to only one initial incision with the model subsequently left to evolve on its own. In the case of a continued incision, normal faults propagated far upslope from the valley flanks. In models having no permanent incision, the contractional downslope buttress eventually blocked further sliding, unless, when the slope was steep, the entire cover started sliding rigidly in a manner similar to systems without incision. In nature, these different evolutionary patterns may depend on local Earth's surface processes, such as continuous or seasonal rainfall. Another process that could be responsible for episodic, rather than continuous, sliding is the sudden loss of fluid pressure during a sliding episode. In such a case, it would take some time for the pressure to build up again beneath the *décollement* layer.

The structural style of models subjected to continuous incision may explain morphostructural observations made onshore, in the Waitawhiti area, where combined river incision and rising thermogenic fluids are observed. However, this combined effect may be applicable to other settings, particularly offshore. There, the influence of fluid overpressure has already been observed. But, in addition, any process that can reduce or remove entirely the downslope buttress could contribute significantly to promoting slides. Such processes could be erosion along submarine canyons, or normal faulting that exposes the *décollement* layer along the fault scarp.

Finally, more work will be needed to characterize and quantify the respective contribution of these two processes by combining in-situ monitoring of sliding events and fluid pressure, and by numerical modelling.

Acknowledgments

We deeply thank William Dunne, Michel Jaboyedoff and José Miguel Azañon, whose very constructive reviews allowed us to strengthen this contribution.

References

Azañon, J.M., Azor, A., Vicente Pérez-Peña, J., Carrillo, J.M., 2005. Late quaternary large-scale rotational slides induced by river incision: the Arroyo de Gor area (Guadix basin, SE Spain). Geomorphology 69, 152–168.

Bayon, G., Loncke, L., Dupré, S., Caprais, J.C., Ducassou, E., Duperron, S., Etoubleau, J., Foucher, J.P., Fouquet, Y., Gontharet, S., Henderson, G.M., Huguen, C., Klaucke, I., Mascle, J., Migeon, S., Ondréas, H., Pierre, C., Sibuet, M., Stadnitsakaia, A., Woodside, J., 2009. In situ investigation of the centre Nile margin: Linking fluid seepage and continental-slope instabilities. Marine Geology 261, 92–104.

Binet, S., Mudry, J., Scavia, C., Campus, S., Bertrand, C., Guglielmi, Y., 2007. In situ characterization of flows in a fractured unstable slope. Geomorphology 86, 193–203.

Chen, H., Dadson, S., Chi, Y.-G., 2006. Recent rainfall-induced landslides and debris flow in northern Taiwan. Geomorphology 77, 112–125.

Cobbold, P.R., Mourgues, R., Boyd, K., 2004. Mechanism of thin-skinned detachment in the Amazon fan: assessing the importance of fluid overpressure and hydrocarbon generation. Marine and Petroleum Geology 21, 1013–1025.

Gay, A., Lopez, M., Cochonat, P., Sermondadaz, G., 2004. Polygonal faults–furrows system related to early stages of compaction - upper Miocene to present sediments of the lower Congo basin. Basin Research 16, 101–116.

Hooper, R.J., Fitzsimmons, R.J., Grant, N., Vendeville, B.C., 2002. The role of deformation in controlling depositional patterns in the south-central Niger Delta, West Africa. Journal of Structural Geology 24, 847–859.

Hovland, M., Gardner, J.V., Judd, A.G., 2002. The significance of pockmarks to understanding fluid flow processes and geohazards. Geofluids 2, 127–136.

Hubbert, M.K., 1937. Theory of scale models as applied to the study of geologic structures. Geological Society of America Bulletin 48, 1459–1520.

Hubbert, M.K., Rubey, W.W., 1959. Role of fluid pressure in mechanics of overthrust faulting. Mechanics of fluid-filled porous solids and its application to overthrust faulting. Geological Society of America Bulletin 70, 115–166.

Kvalstad, T.J., Andresena, L., Forsberga, C.F., Bergb, K., Brynb, P., Wangen, M., 2005. The Storegga slide: evaluation of triggering sources and slide mechanics. Marine and Petroleum Geology 22, 245–256.

Lacoste, A., Loncke, L., Chanier, F., Bailleul, J., Vendeville, B.C., Mahieux, G., 2009. Morphology and structure of a landslide complex in an active margin setting: The Waitawhiti complex, North Island, New Zealand. Geomorphology 109, 184–196.

Lastras, G., Canals, M., Urgeles, R., Hughes-Clarke, J.-E., Acosta, J., 2004. Shallow slides and pockmark swarms in the Eivissia channel, western Mediterranean sea. Sedimentology 51, 1–14.

Loncke, L., Mascle, J., Fanil Science Party, 2004. Mud volcanoes, gas chimneys pockmarks and ridges in the Nile deep-sea fan (eastern Mediterranean): geophysical evidences. Marine and Petroleum Geology 21, 669–689.

Mourgues, R., Cobbold, P.R., 2003. Some tectonic consequences of fluid overpressures and seepage forces as demonstrated by sandbox modelling. Tectonophysics 376, 75–97.

Mourgues, R., Cobbold, P.R., 2006. Sandbox experiments on gravitational spreading and gliding in the presence of fluid overpressures. Journal of Structural Geology 28, 887–901.

Osborne, M.J., Swarbrick, R.E., 1997. Mechanisms for generating overpressure in sedimentary basins: A reevaluation. American Association of Petroleum Geologists 81 (6), 1023–1041.

Ramberg, H., 1981. Gravity, Deformation and the Earth's Crust: In Theory, Experiments and Geological Application, second ed.. Academic Press, London and New York, 452 pp.

Schultz-Ela, D.D., Walsh, P., 2002. Modeling grabens extending above evaporites in Canyonlands national park, Utah. Journal of Structural Geology 24, 247–275.

Shuzui, H., 2001. Process of slip-surface development and formation of slip-surface clay in landslides in tertiary volcanic rocks, Japan. Engineering Geology 61, 199–219.

Sultan, N., Cochonat, P., Cayocca, F., Bourillet, J.-F., Colliat, J.-L., 2004. Analysis of submarine slumping in the Gabon continental slope. American Association of Petroleum Geologists 88, 781–799.

Terzaghi, K.v., 1923. Die Berechnung der Durchlässigkeitsziffer des tones aus dem Verlauf der hydrodynamischen Spannungerscheinungen. Akademie der Wissenschaften in Wien. Sitzungsberichte, Mathematisch-Naturwissenschaftliche Klasse - IIa 132, 125–138.

Terzaghi, K.v., 1959. Soil mechanics in action. Civil Engineering 29, 69–70.

Trincardi, F., Cattaneo, A., Correggiari, A., Ridente, D., 2004. Evidence of soft sediment deformation, fluid escape, sediment failure and regional weak layers within the late quaternary mud deposits of the Adriatic sea. Marine Geology 213, 91–119.

Weber, K.J., Daukoru, E.M., 1975. Petroleum Geology of the Niger Delta: Proceedings of the Ninth World Petroleum Congress. Geology, vol. 2. Applied Science Publishers, Ltd., London, pp. 210–221.